



Means of Enhancing the Power Output and Widening the Operational Frequency Band of Vibration-Based Electromagnetic Energy Harvester

Vijay B. Patil¹ · Rajendra S. Kattimani² · Mahadev Sakri² · Pradeep V. Malaji²

Received: 20 December 2022 / Revised: 20 May 2023 / Accepted: 30 July 2023 / Published online: 24 August 2023
© Krishtel eMaging Solutions Private Limited 2023

Abstract

Purpose This paper presents the design, development, and performance analysis of a Two-Degree-of-Freedom Vibration-Based Electromagnetic Energy Harvester (TDOF VBEEH). The purpose is to enhance power output and widen the operational frequency band of the harvester. In the literature, various techniques such as mechanical amplification, resonance tuning, and nonlinear oscillations etc., have been explored. The proposed TDOF VBEEH incorporates a mechanical amplifier in series with a traditional Single-Degree-of-Freedom (SDOF) VBEEH.

Methods The paper derives an analytical expression for the average power output of the TDOF VBEEH based on the principles established by Tang and Zuo. The effects of mass ratio, electrical damping ratio, and tuning ratio on the power output and effective operational frequency band of TDOF VBEEH have been studied to provide design guidelines for TDOF VBEEH. Also, the experimental analysis is conducted to examine the effects of a purely resistive load and mass ratio on the average harvested power of the TDOF VBEEH. The study utilizes a specially designed setup for TDOF VBEEH. Furthermore, by employing the method of surface plots and contour diagrams, the global optimum values of power output for the TDOF VBEEH under various electrical damping ratios and normalized excitation frequencies have been determined.

Results The results demonstrate that the appropriate selection of mass ratio, tuning ratio, and electrical damping ratio can enhance the power output and widen the effective operational frequency band of the TDOF VBEEH. Notably, the maximum harvested power is achieved when the electrical circuit connected to the harvester has a resistive load of approximately 1500 Ω , which aligns with the internal resistance of the copper coil. The results show that the increased power output is attainable over a widened operational excitation frequency band compared to the traditional Single-Degree-of-Freedom (SDOF) VBEEH. From the comparison of the experimental and analytical results, it is seen that the TDOF VBEEH performs better than the SDOF VBEEH when the parameters are properly chosen.

Conclusion These findings highlight the superior performance and potential of TDOF VBEEHs over SDOF VBEEHs, emphasizing the importance of parameter selection in maximizing power output and widening the operational frequency band. Also, the findings offer valuable design guidelines for selecting system parameters when developing TDOF VBEEHs to power small electronic devices.

Keywords Electromagnetic energy harvester · Electrical damping ratio · Mass ratio · Tuning ratio

✉ Pradeep V. Malaji
pradeepmalaji@bldeacet.ac.in

Vijay B. Patil
vijaypatil2005@rediffmail.com

Rajendra S. Kattimani
mech.kattimani@bldeacet.ac.in

Mahadev Sakri
mech.sakri@bldeacet.ac.in

¹ Mechanical Engineering Department, Annasaheb Dange College of Engineering and Technology, Tal:-Walwa, Dist.:-Sangli, Ashta, Maharashtra 416301, India

² Vibration Energy Harvesting and IoT Laboratory, Mechanical Engineering Department, BLDEAs V.P.Dr.P.G.Halakatti College of Engineering and Technology, Vijayapur 586101, India

Introduction

In the last few decades, scientists and engineering researchers have been working on seeking solutions to the problem of the development of uninterrupted maintenance-free power sources for small electronic devices in general and remotely located wireless sensor nodes in particular. The development of a single degree of freedom (SDOF) vibration-based electromagnetic energy harvester (VBEEH) has come up as a satisfactory solution to this problem. SDOF VBEEHs are reliable, simple in construction and have huge design flexibility, and can be made available in small sizes and weights. However, this harvester gives maximum power output only at the resonant frequency and its effective operational frequency band is extremely narrow. Therefore, engineers—designers—researchers have proposed some innovative methods to enhance the power output and widen the operational frequency band. An excellent survey of electromagnetic electrostatic, piezoelectric and magnetoelectric [1–3], with vibration-based energy harvesting technology, hybrid mechanism [4] and architectural approach has been presented by various researchers [4–6]. Patil and Sakri [7] have shown that the maximum attainable power generated from a VBEEH is significantly influenced by the values of the mechanical damping ratio, during resonance and off-resonance conditions. From the results of theoretical and experimental investigation for optimal power output from VBEEH, the mechanical damping ratio should be as low as possible and the electrical damping ratio should be almost equal to the mechanical damping ratio. They have also studied experimentally the effect of shunted electrical loads on the performance of a VBEEH. Halim et al. [8, 9] have shown that the electrical damping ratio may be adjusted by varying the resistive load to achieve the maximum power output. The damping characteristics of the electromagnetic harvester system are determined by using an impulse response. Zhang et al. [10] investigated the effect of ohmic resistors, rectifiers, and capacitors on electromagnetic harvester performance. The main challenge to be addressed in adopting VBEEH is to increase its output voltage. VBEEHs in general have a very low voltage (piezoelectric, electromagnetic or electrostatic) only at one or a few excitation frequencies. Hence, the resonance generator produces maximum power when excited at its resonant frequency. Yildirim et al. [11] have reviewed the performance enhancement methods such as power amplification, resonance tuning, and means for increasing the effective operating bandwidth of a vibration energy harvester, and presented a summary of these methods with their merits and limitations, using different approaches such as the design of broadband frequency VBEEHs [12, 13], tunable frequency VBEEHs [14], nonlinear resonance [15] (dynamic magnifier [16, 17] and frequency up-conversion methods [18]). Malaji et al. [19, 20] presented the

methods of enhancing the energy harvesting capability of coupled harvesters suitable for low-frequency applications. They have also proposed the multiple harvesters with intentional mistuning to obtain the wider bandwidth. Chaurha et al. [21] have reported a method of enhancement of bandwidth and vibration suppression of energy harvester using the nonlinear attachments. Chen and Wu [22] have presented a two degree of freedom electromagnetic energy harvester to increase the operating frequency bandwidth by incorporating a spiral diaphragm into a U-shaped cantilever. Tao et al. [23] have presented a novel two degree of freedom MEMS electromagnetic vibration energy harvester to address the fundamental issue of these energy harvesters that they give maximum power output in a narrow bandwidth around the resonance frequency of the ambient mechanical vibration sources which have distributed/multiple frequencies. Tang and Zuo [24] have proposed a dual-mass vibration energy harvester to obtain a higher energy harvesting rate and have shown that the local maximum power of the proposed harvester is larger than the global maximum power of the traditional single degree of freedom vibration energy harvester. Also, the parameters of the dual-mass energy harvester have been optimized, which maximize the energy harvesting capability of the dual-mass vibration energy harvester when subjected to harmonic excitation. Tai and Zuo [25] have obtained the condition for optimization for maximum power output from vibration-driven electromagnetic and piezoelectric energy harvester devices. These conditions have been derived by using resistive load, electrical damping ratio, and the normalized excitation frequency. Smilek and Hadas [26] have shown the performance enhancement of electromagnetic energy harvester is possible by maximizing electromechanical coupling by optimization of magnetic circuit design, placement of coil, its shape and size. Kim et al. [27] have proposed an approach for optimizing voltage and power from three different types of vibration-driven electromagnetic vibration energy harvesters having the same volume. Maroofiazar and Farzam [28] have carried out numerical modeling, statistical analysis and experimental investigation of a hybrid energy harvester. For the experimental investigation, the system is prepared by floating a magnet coiled fluid container subjected to vibrations peak to peak values of voltage and electrical power obtained are 740 mW and 58 μ W, respectively. Wang et al. [29] have proposed a method of scavenging vibrational energy from ultra-low-frequency vibrations with low excitation levels. In the proposed electromagnetic energy harvester, a rolling magnet system has been used. An analytical solution of this harvester performs has been derived. The realistic ambient vibration accelerations from a bus and human body are applied to excite to this harvester. Researchers have also started to explore self-powered active vibration control technologies. Such dual degree systems can also be used

to control the vibrations [21]. In recent years, active vibration control based on boundary control has been greatly developed, these type of harvesters can used in such cases such as Boundary Control of a Rotating and Length-Varying Flexible Robotic Manipulator System [30], Modeling and Observer-Based Vibration Control of a Flexible Spacecraft With External Disturbances and Asymmetric Input–Output Constraint Control of a Flexible Variable-Length Rotary Crane Arm [31].

The contribution of this paper lies in proposing a practical setup for a Two-Degree-of-Freedom (TDOF) Vibration-Based Electromagnetic Energy Harvester (VBEEH) and providing both theoretical and experimental analysis of its performance. While existing literature primarily focuses on theoretical analyses of TDOF systems, with only a few incorporating experimental studies, this paper bridges the gap by presenting tangible results. The paper begins by deriving an expression for the maximum average power generated by a TDOF VBEEH, employing the approach proposed by Tang and Zuo [24]. This theoretical analysis sets the foundation for understanding the power output capabilities of the TDOF system. To validate the theoretical findings, an experimental setup is designed and developed specifically for studying the effect of varying mass ratios and electrical resistive loads on the harvested power of the TDOF VBEEH. This experimental analysis provides practical insights into the performance of the TDOF system and allows for a comprehensive evaluation of its power output under different conditions. By combining theoretical derivation and experimental validation, this paper offers a comprehensive understanding of the TDOF VBEEH and its capabilities. The proposed practical setup enhances the applicability of the research, allowing for practical implementation and validating the theoretical predictions. This holistic approach contributes to the body of knowledge surrounding TDOF VBEEHs and facilitates further advancements in the field.

Analysis of Single Degree of Freedom (SDoF) and Two Degree of Freedom (TDoF) Harvesters

This section analyses the single degree of freedom (SDoF) and two degrees of freedom (TDOF) vibration energy harvesters subjected to base excitation as shown in Fig. 1. The SDoF harvester consists of mass m_2 , spring k_2 , damper c and energy transducer with load resistance R_h as shown in Fig. 1a. Figure 1b shows the TDoF harvester by connecting additional mass m_1 and spring k_1 between base and harvester setup.

The governing equation for SDoF harvester under base excitation $x_0 = X\sin\omega t$, where, ω and X_0 are, respectively, the circular excitation frequency and amplitude of ambient vibration is given as.

$$m\ddot{z} + c\dot{z} + kz + f_e = m\ddot{x}_0, \quad f_e = \frac{k_t k_e \dot{z}}{R_h}, \tag{1}$$

where Z is the relative motion ($x_2 - x_0$), f_e is the force provided by the energy transducer [24], k_t is thrust motor constant, k_e is back EMF, R_h is load resistance. The damping coefficient consists of both mechanical and electrical component $c = c_m + c_e$.

The steady-state amplitude Z and using $\zeta_m = \frac{c}{2\sqrt{mk}}$, $\zeta_e = \frac{c_e}{2\sqrt{mk}}$, $\omega_n = \sqrt{\frac{k}{m}}$ will be

$$|Z| = \frac{\left(\frac{\omega}{\omega_n}\right)^2 X}{\sqrt{\left(1 - \left(\frac{\omega}{\omega_n}\right)^2\right)^2 + \left(2(\zeta_e + \zeta_m)\left(\frac{\omega}{\omega_n}\right)\right)^2}} \tag{2}$$

The average power output from a single degree of freedom (SDoF) VBEEH is given as,

$$P_{ave} = \frac{1}{2} c_e \dot{z}^2, \tag{3}$$

$$P_{ave} = \frac{m_2 \omega^3 X^2 \zeta_e \left(\frac{\omega}{\omega_2}\right)^3}{\left(1 - \left(\frac{\omega}{\omega_2}\right)^2\right)^2 + \left(2(\zeta_e + \zeta_m)\frac{\omega}{\omega_2}\right)^2} \tag{4}$$

The non-dimensional form of P_{ave} is denoted as P_{aven} and is given as

$$P_{aven} = \frac{P_{ave}}{m_2 \omega^3 X_0^2} = \frac{\zeta_e(\alpha)^3}{(1 - (\alpha)^2)^2 + (2(\zeta_e + \zeta_m)\alpha)^2} \tag{5}$$

The equations of motion for TDoF system is given as,

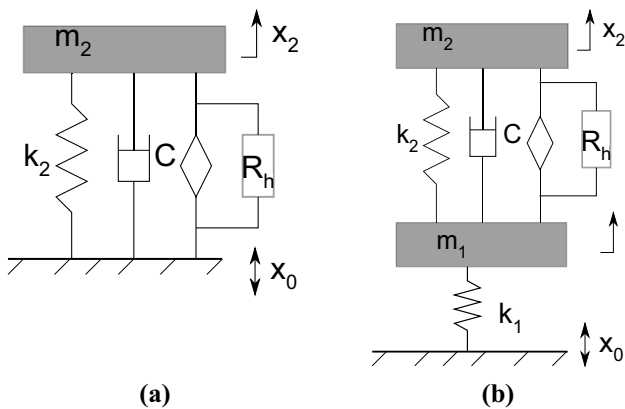


Fig. 1 Schematic of harvesters a SDoF, b TDoF

$$\begin{aligned}
 m_2 \ddot{x}_2 &= -k_2(x_2 - x_1) - c(\dot{x}_2 - \dot{x}_1) + f_e \\
 m_1 \ddot{x}_1 + f_e &= -k_2(x_1 - x_2) - c(\dot{x}_1 - \dot{x}_2) - k_1(x_1 - x_0).
 \end{aligned}
 \tag{6}$$

The relative displacement z between mass m_2 and mass m_1 is $z = x_2 - x_1$

$$\begin{aligned}
 m_2 \ddot{z} + k_2 z + c \dot{z} &= -m_2 \ddot{x}_1 \\
 m_1 \ddot{x}_1 + k_1 x_1 - k_2 z - c \dot{z} - k_1 x_0 &= 0.
 \end{aligned}
 \tag{7}$$

The non-dimensional output power $\overline{P_{\text{aven}}}$ of 2DOF VBEEH as

$$\overline{P_{\text{aven}}} = \frac{\zeta_e \mu f \alpha^6}{[\alpha^4 + f^2 - (1 + (1 + \mu)f^2)\alpha^2]^2 + 4(\zeta_e + \zeta_m)^2 [f\alpha - (1 + \mu)f\alpha^3]^2},
 \tag{8}$$

where mass ratio $\mu = \frac{m_2}{m_1}$, Tuning ratio $f = \frac{\omega_s}{\omega_1}$, and frequency ratio $\alpha = \frac{\omega}{\omega_1}$. The detailed derivations are given in Appendix-1.

Figure 2a shows the variation of non-dimensional power Paven with excitation frequency α for various mass ratios μ of TDoF and SDoF. The tuning ratio f is kept at 1. The TDoF harvester can harvest power at two different peaks as compared to SDoF harvester indicating possibility of enhanced frequency bandwidth. The non-dimensional peak power of SDoF harvester is 2.4 it is further enhanced when a TDoF harvester is considered. Figure 2c shows the variation in non-dimensional peak power SDoF and TDoF at various mass ratios. An increase of 50–100% increase in peak power can be achieved when mass ratio μ is varied between 0.05

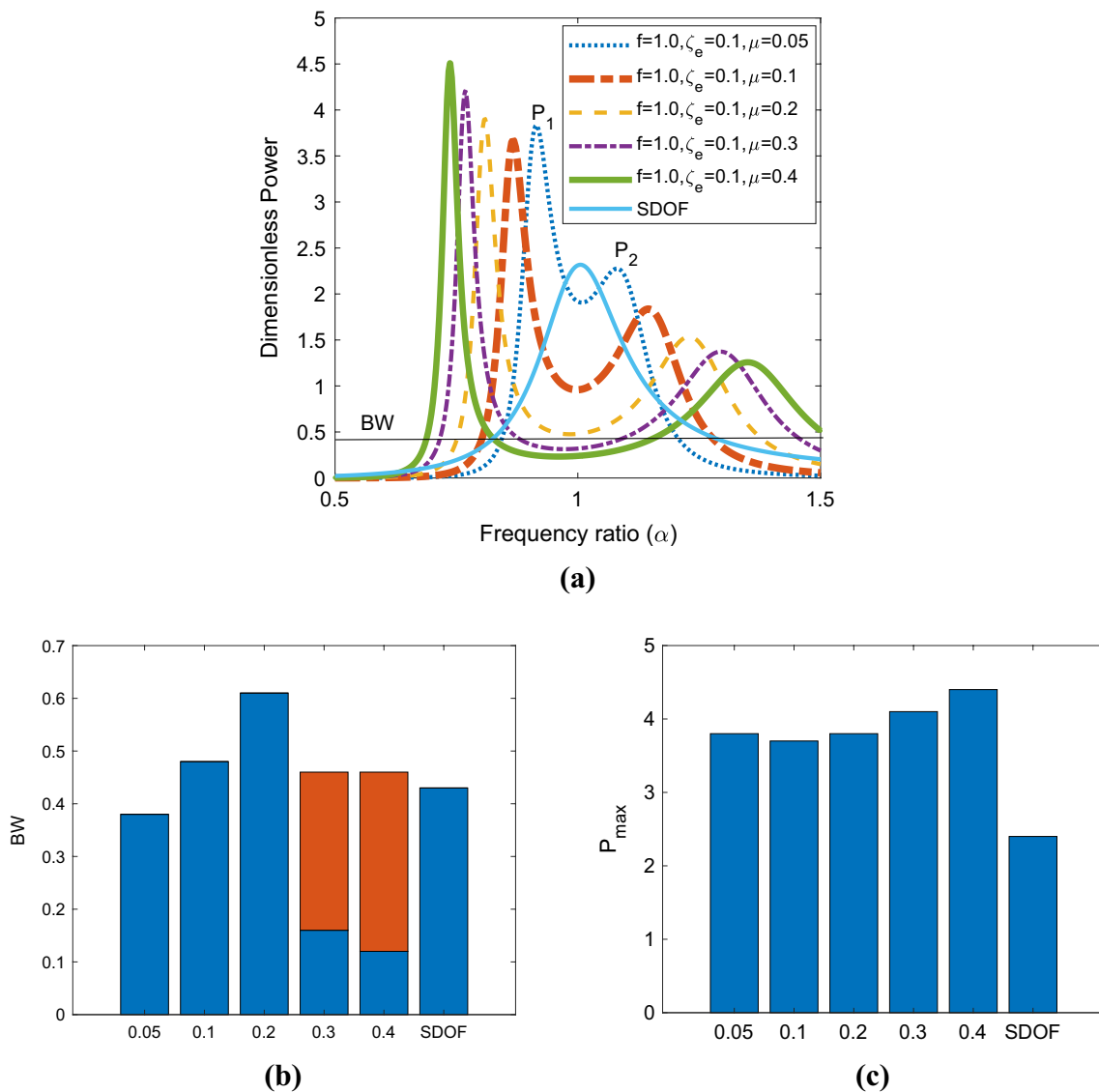


Fig. 2 Comparison of SDoF and TDoF with different mass ratios **a** Power curve, **b** Frequency bandwidth, **c** Maximum power harvested (BW-frequency bandwidth)

and 0.4. The frequency band width is measured at 20% of peak power of SDoF ($P_{\max}=0.48$) marked as BW in Fig. 2a. The variation of bandwidth is shown in Fig. 2b SDoF has a bandwidth of 0.43 and TDoF with mass ratio $\mu=0.05$ has a bandwidth of 0.38 indicating a small decrease in bandwidth. The bandwidth of TDoF increases with increase in mass ratio and attains a high value of 0.61 at $\mu=0.2$. The bandwidth is split in to two bands when μ is 0.3 and 0.4 around two different modes. It is also observed that with increase in mass ratio the distance between two peaks (P_1 and P_2) increases reducing the effective bandwidth.

To study the effect of mass ratio and tuning ratio on frequencies, the electrical sub-system from TDoF is removed and assume that the mechanical damping and electrical damping as zero i.e $\zeta_m = \zeta_e = 0$. The expression for non-dimensional first mode frequency $\overline{\omega}_{n1}$ and non-dimensional second mode frequency $\overline{\omega}_{n2}$ have been obtained using well founded theory of vibration. These expressions are as follows; we get, non-dimensional first mode frequency $\overline{\omega}_{n1}$, as

$$\overline{\omega}_{n1} = \sqrt{\frac{[1 + (1 + \mu)f^2]}{2}} - \sqrt{\left[\frac{[1 + (1 + \mu)f^2]}{2}\right]^2 - f^2}. \tag{9}$$

Non-dimensional second mode frequency $\overline{\omega}_{n2}$, as

$$\overline{\omega}_{n2} = \sqrt{\frac{[1 + (1 + \mu)f^2]}{2}} + \sqrt{\left[\frac{[1 + (1 + \mu)f^2]}{2}\right]^2 - f^2}. \tag{10}$$

The detailed expressions are given in Appendix II.

The variation of natural frequencies $\overline{\omega}_{n1}$ and $\overline{\omega}_{n2}$ vs. μ for cases $f=1.0$, and 0.8 are shown Fig. 3a and b. The distance between $\overline{\omega}_{n1}$ and $\overline{\omega}_{n2}$ increase with increase in mass ratio μ indicating increased distance between two peak powers P_1 and P_2 and decrease in bandwidth as shown in Fig. 2a. The variation in peak powers P_1 and P_2 with mass ratio μ is shown in Fig. 3c. The peak P_1 keeps on increasing and P_2 keeps on decreasing with increase in mass ratio μ . Hence, with increase in μ there is decrease in peak P_2 and it

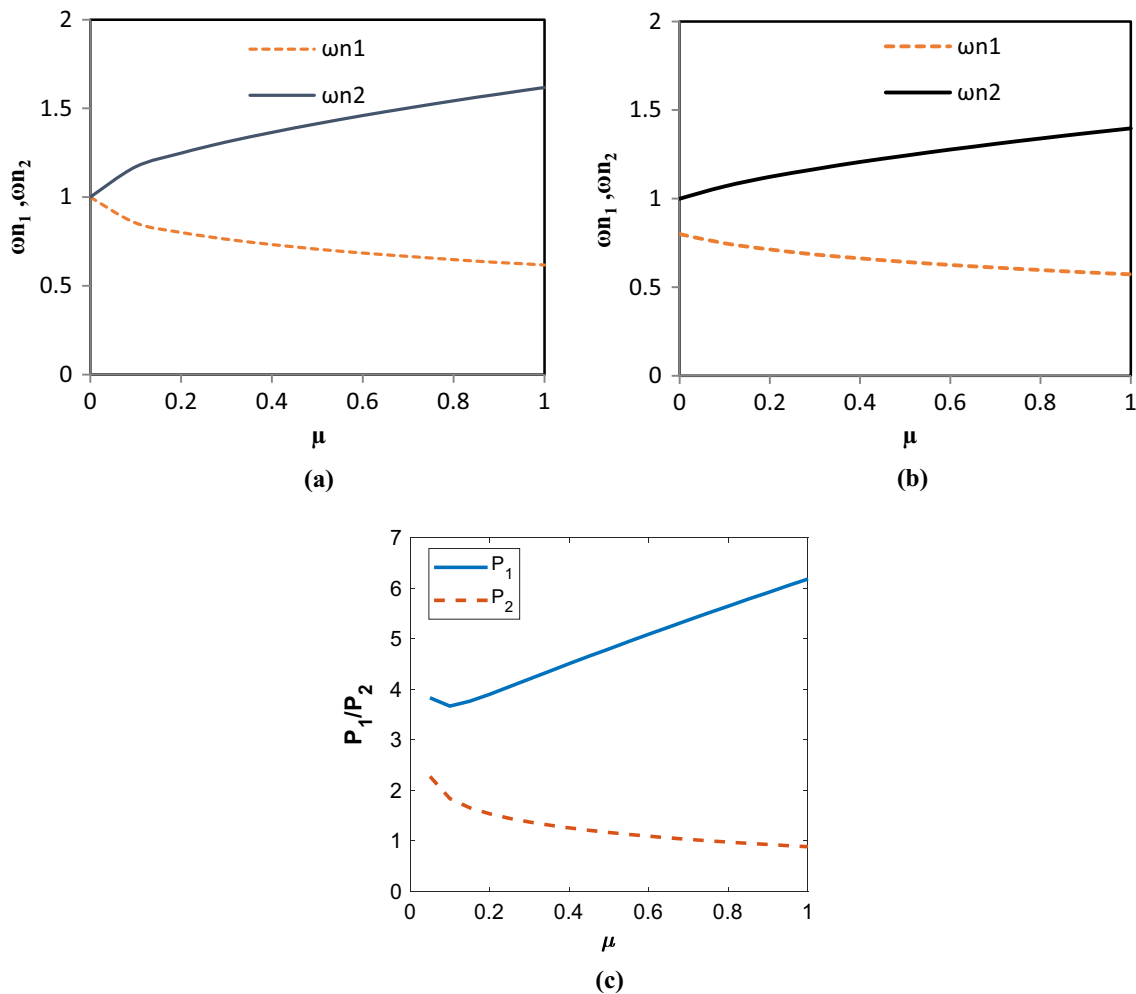


Fig. 3 Effect of μ on $\overline{\omega}_{n1}$ and $\overline{\omega}_{n2}$ **a** $f=1.0$, **b** $f=0.8$, **c** effect on P_1 and P_2 $f=1$

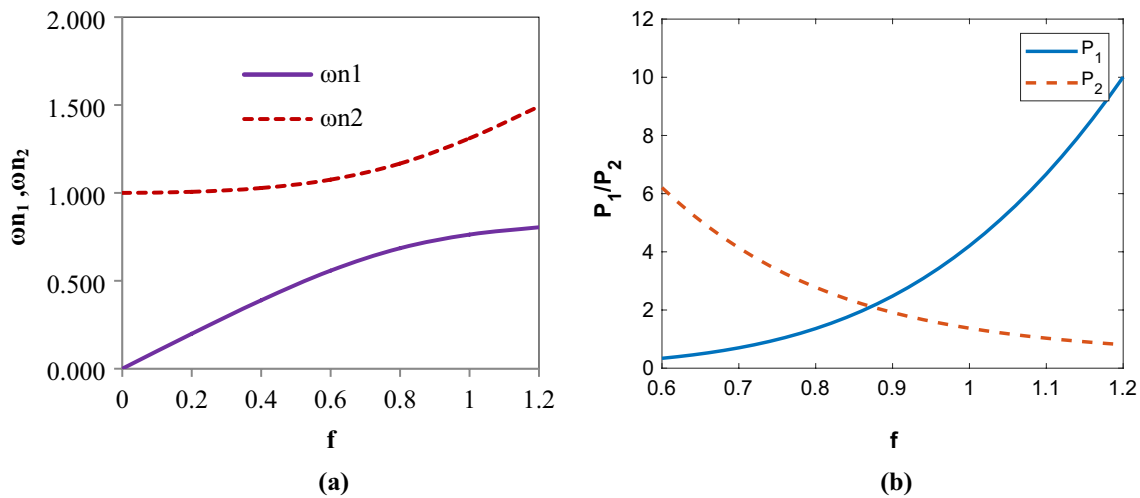


Fig. 4 **a** Effect of f on $\overline{\omega_{n1}}$ and $\overline{\omega_{n2}}$ $\mu=0.3$, **b** effect on P_1 and P_2 $\mu=0.3$

occurs away from P_1 , it leads to the reduction in bandwidth. Therefore, peaks should neither be too close or too far to obtain better band width. The optimum mass ratio seems to be 0.2–0.4 for better power output and bandwidth.

The variation of $\overline{\omega_{n1}}$ and $\overline{\omega_{n2}}$ with tuning ratio f , for $\mu=0.3$ is shown in Fig. 4a. From Fig. 4a, b, it is seen that as the values of tuning ratio f increases, the first mode natural frequency $\overline{\omega_{n1}}$ decreases initially and increases thereafter, reverse trend is followed by the second mode natural frequency $\overline{\omega_{n2}}$. The values of P_1 and P_2 are equal when $f = \sqrt{\frac{1}{1+\mu}}$ [24], for $f < \sqrt{\frac{1}{1+\mu}}$ P_2 is greater than P_1 reverse happens when $f > \sqrt{\frac{1}{1+\mu}}$. To get maximum power output and better bandwidth, the tuning ratio $f=1$.

The power output of 2DOF VBEEH is influenced by four major parameters, viz., the electrical damping ratio ξ_e , mass ratio μ , the tuning ratio f , and the excitation frequency ratio α . The power output of 2DOF VBEEH obtained by applying a single variable optimization technique will be an optimal value of P_{ave} with respect to that variable only and may not be of the same value for the optimal value of P_{ave} obtained for other variables such as mass ratio μ . As such, the problem here is to obtain global optimal value of output power P_{ave} of TDOF VBEEH when ξ_e and α are varied simultaneously for a set of values of tuning ratio $f=0.8$, $f=1.0$ and $f=1.2$, and for a given value of μ or a set of values of mass ratio, $\mu=0.1$, and $\mu=0.3$ for a given value of tuning ratio f . To achieve this goal, the method of drawing surface plots and contour diagrams has been used to obtain global optimal value of power output of a TDOF VBEEH device. The details of drawing these plots are presented in the sections to follow. From these plots, the global optimal non-dimensional value of power output P_{aven} under a given set of conditions can be obtained.

It can be seen from Eq. 11, that the value of $\overline{P_{aven}}$ is controlled by mass ratio μ , tuning ratio f , frequency ratio α , and electrical damping ratio ξ_e .

Using the theoretical Eq. 8 for non-dimensional average power output $\overline{P_{aven}}$ from a 2DOF VBEEH and associated variables which control the value of $\overline{P_{aven}}$, MATLAB has been used to draw surface plots and contour diagram.

- (i) The resulting surface plots showing the non-dimensional average power output $\overline{P_{aven}}$ with respect to normalized excitation frequency α , at various values of electrical damping ratio ξ_e for given value of mass ratio μ are shown in Fig. 5 for tuning ratio $f=1$, Fig. 6 for $f=0.8$, and Fig. 7 for $f=1.2$.

Case I: $f=1.0$. From Fig. 5, it is seen that $\overline{P_{aven}}$ increases with the increase in value of ξ_e for $\mu=0.1$. The value of $\overline{P_{aven}}$ is at maximum at first mode resonant frequency α_1 of TDOF VBEEH as shown in Fig. 5a and c. The case $\mu=0.3$ and $\xi_e=0.1$ gives a better compromise between the maximum value of $\overline{P_{aven}}$ and bandwidth as shown in Fig. 5b and d.

Case II: $f=0.8$. From Fig. 6, it can be seen that for small values of μ and ξ_e the maximum value $\overline{P_{aven}}$ occurs almost at the second normalized resonant frequency α_2 of TDOF VBEEH, however, the bandwidth is less than that for the case $f=1.0$.

Case III: $f=1.2$. From Fig. 7, it can be seen that for the values of $\mu=0.1$, and 0.3, for small values of ξ_e , almost all the non-dimensional power output $\overline{P_{aven}}$ of the TDOF VBEEH occurs at the first mode resonant normalized excitation frequency α_1 . The value of $\overline{P_{aven}}$, in this case is the highest with extremely narrow bandwidth i.e. in the neighborhood of first mode natural frequency α_1 .

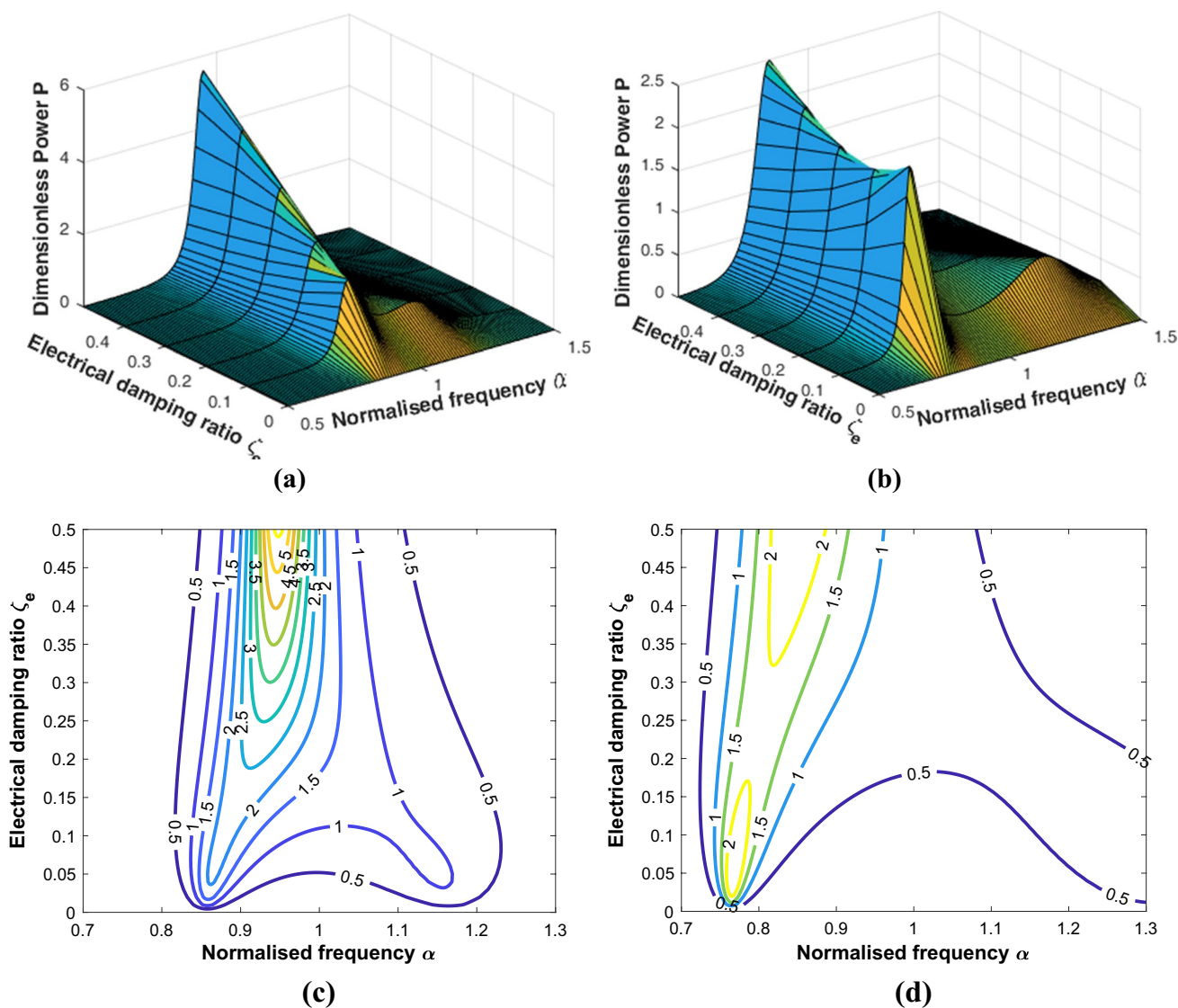


Fig. 5 The power output P_{aven} of 2DOF VBEEH at different values of excitation frequencies α and electrical damping ratios ζ_e , $f=1$ and $\zeta_m = 0.046$ when, **a, c** $\mu=0.1$, **b, d** $\mu=0.3$

Experimental Analysis

In this section, experimental analysis of SDoF and YdoF vibration energy is presented.

The Experimental setup has been designed in such a way that the SDOF VBEEH system can be converted to a 2DOF VBEEH with a little bit of a change in the setup.

The experimental setup designed and developed for 2 DOF VBEEH is shown in Fig. 8. The system (m_2, k_2, c_m, c_e) is the energy harvester. The helical compression spring of stiffness k_2 is split into two springs of equal stiffness $\frac{k_2}{2}$ and these springs are placed in parallel to support the harvester mass m_2 . The system (m_1, k_1) is the amplifier system. The

mass m_2 is supported by helical compression springs each of stiffness $\frac{k_1}{2}$ and are placed in parallel.

The rectangular plates of appropriate size are selected to represent harvester mass m_2 , amplifier mass m_1 , and the base plate. The base plate supports the amplifier system. All the plates are equipped with rolling contact bearings to ensure frictionless movement of these plates in the vertical direction in the two vertical parallel guide bars. The cam is driven by an electrical drive motor and is mounted at the end of the electrical drive motor shaft. The guide bars are mounted firmly in the foundation.

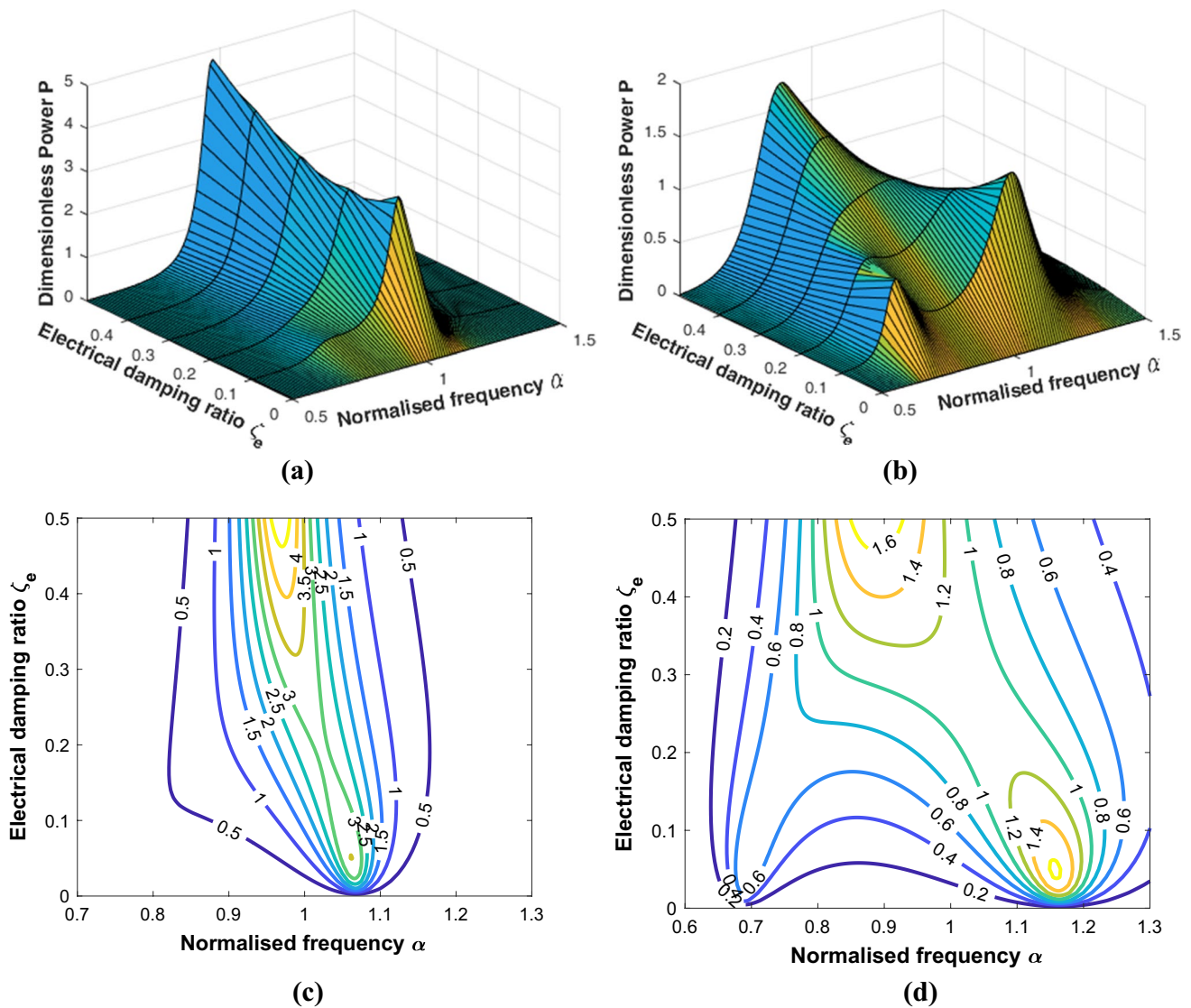


Fig. 6 The power output P_{aven} of 2DOF VBEEH at different values of excitation frequencies α and electrical damping ratios ζ_e , $f=0.8$ and $\zeta_m = 0.046$ when, **a, c** $\mu=0.1$, **b, d** $\mu=0.3$

Electrical Copper Coil Magnet Sub-system

The coil-magnet system comprises of a ‘Magnet-in-line’ type configuration in which a cylindrical magnet moves in the vertical direction in an electrical coil of copper material. Figure 14 (appendix III) shows the magnet to be fixed to the harvester mass plate and the copper coil to be fixed to the amplifier mass plate with proper alignment in vertical direction. The relative movement between magnet and coil provides a magnetic field which when cut gives rise to an electromotive force.

Selection of Magnet and Coil Design

The method of selecting the magnet and design calculation for coil for magnet-coil sub-system are given in Appendix III.

Design Calculations

- (i) To increase the power output and to extend the effective operational frequency range of 2 DOF VBEEH device, and to keep its weight low, a reasonable choice for the mass ratio μ is in the range 0.3–0.4, hence for the analysis, the reasonable values of mass ratio μ are taken as 0.3 and 0.36.
- (ii) The VBEEH is designed essentially for low-frequency excitation. Hence, the excitation frequency f_w is taken as 5.5 Hz, therefore, the circular excitation frequency is $\omega = 2\pi f_w = 34.54\text{rad/s}$, for tuning ratio $f = 1$, hence, $\omega_1 = \sqrt{\frac{k_1}{m_1}} = \omega_2 = \sqrt{\frac{k_2}{m_2}} = \omega = 34.54\text{rad/s}$

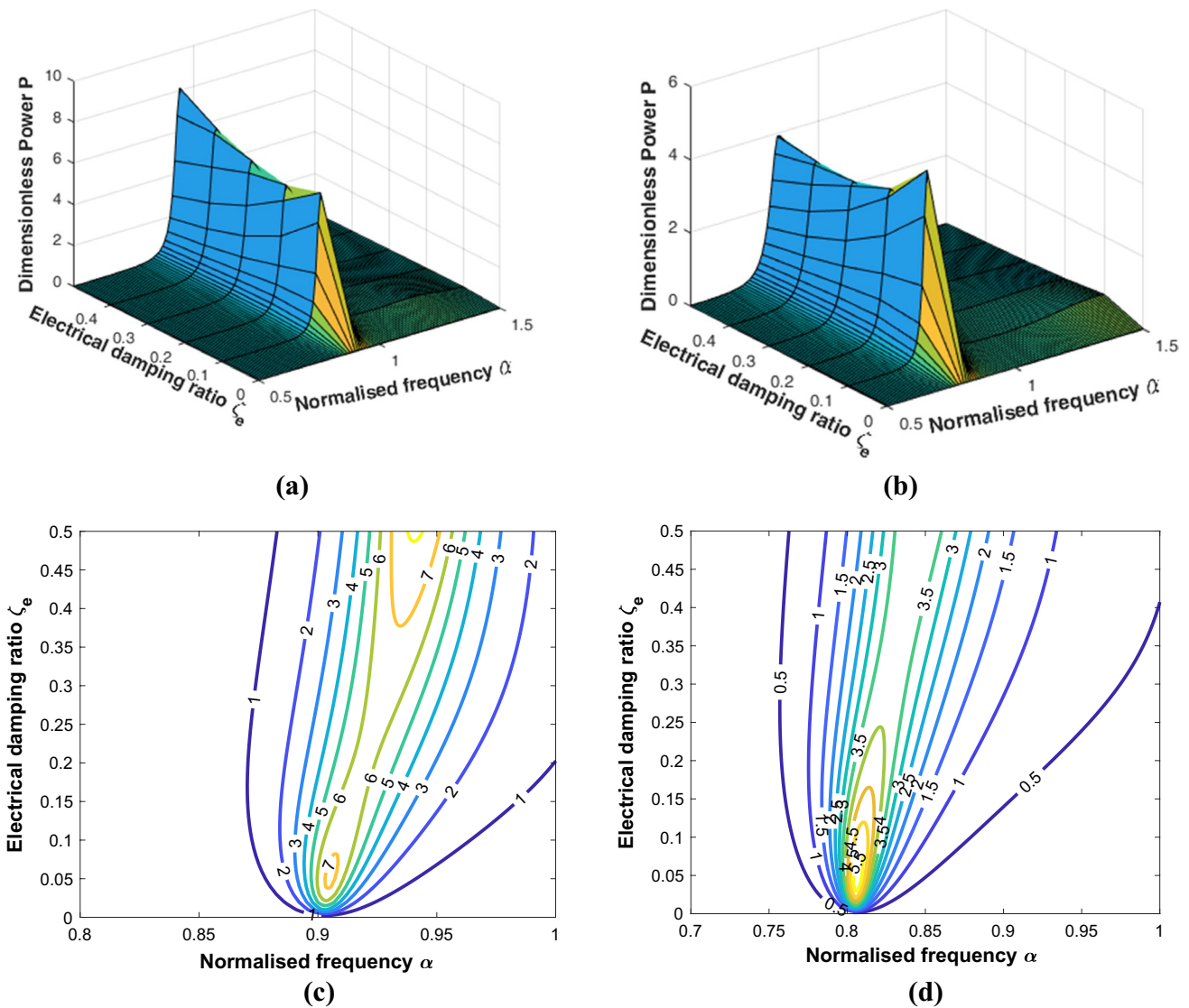


Fig. 7 The power output P_{aven} of 2DOF VBEEH at different values of excitation frequencies α and electrical damping ratios ζ_e , $f=1.2$ and $\zeta_m = 0.046$ when, **a, c** $\mu=0.1$, **b, d** $\mu=0.3$

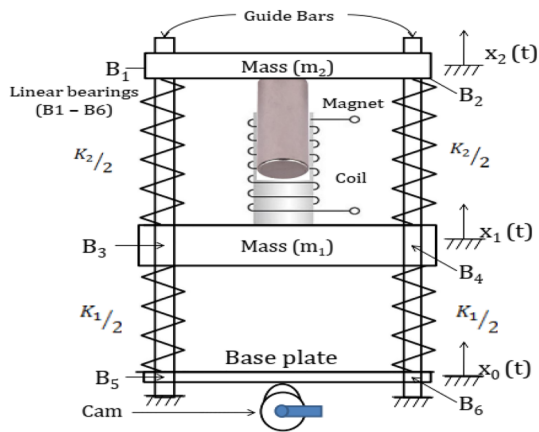


Fig. 8 The schematic and experimental setup of two DOF VBEEH

Sample Calculations for the Case $\mu=0.36$

With the harvester mass $m_2 = 2.4\text{kg}$, the amplifier mass m_1 is $m_1 = \frac{m_2}{\mu} = \frac{2.4}{0.36} = 6.67\text{kg}$. Using equations $\omega_1 = \sqrt{\frac{k_1}{m_1}}$ and $\omega_2 = \sqrt{\frac{k_2}{m_2}}$ and $\omega_2 = \omega_1$ for $f=1$, the values of amplifier spring stiffness k_1 and harvester system spring stiffness k_1 and k_2 are calculated as $k_1 = 7957.38\text{N/m}$ and $k_2 = 2863.22\text{N/m}$. For harvester system, two helical compression springs of stiffness $\frac{k_2}{2}$ are used in parallel. Therefore each of these two springs is designed for stiffness $\frac{k_2}{2} = 1431.6\text{N/m}$, using standard spring design procedure. Amplifier mass is supported by two springs of stiffness $\frac{k_1}{2}$ in parallel, hence each of these springs is designed for stiffness

Table 1 Specifications of the amplifier and harvester springs

| Spring system | Material of the spring | Length of spring (mm) | Wire dia. D (mm) | Mean dia. D (mm) | No. of turns (N) |
|---------------|------------------------|-----------------------|------------------|------------------|------------------|
| Amplifier | Spring steel | 116 | 4.5 | 65 | 7 |
| Harvester | Spring steel | 192 | 4.5 | 65 | 11 |

$\frac{k_1}{2} = 3978.7\text{N/m}$ using standard spring design procedure. Design specifications of these springs are given in Table 1

(iii) Rectangular M.S. plate of size $325 \times 75 \times 15$ mm is selected as the harvester mass m_2 . Refer Fig. 9a and b. The amplifier mass m_1 is made up of 3 rectangular plates of sizes $325 \times 75 \times 12$.

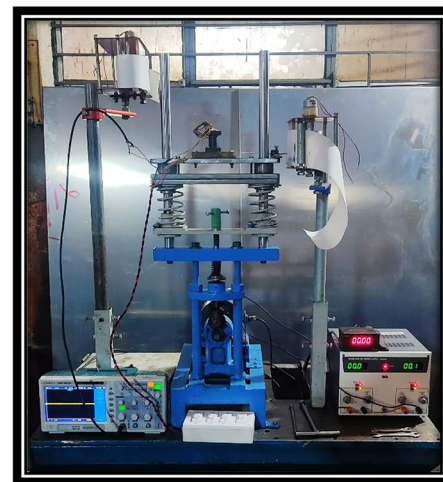
Fig. 9 The developed harvester and amplifier mass



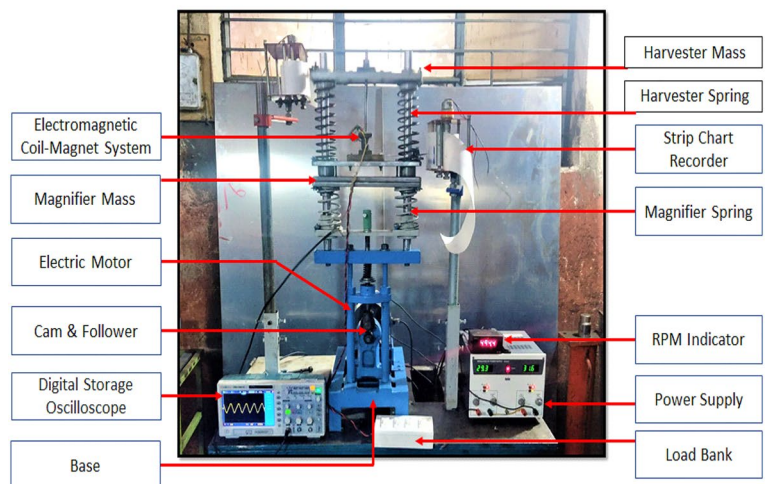
(a) Developed harvester mass

(b) Developed amplifier mass

Fig. 10 Experimental setup and instrumentation for (a) SDOF (b) TdoF VBEEH



(a)



(b)

- (iv) A suitable M.S. plate is selected as a base plate to support amplifier spring-mass system. The base plate receives sinusoidal excitation by a cam driven by variable speed electric motor.

Experimental Analysis

The entire experimental setup with attendant instrumentation for SdoF and TdoF VBEEH is shown in Fig. 10.

Experimental Analysis of SDOF VBEEH System (m_2, k_2, c_m, c_e)

By removing amplifier (m_1, k_1) system from the TDOF VBEEH set-up the SDOF (m_2, k_2, c_m, c_e) VBEEH system is obtained. This SDOF VBEEH system is subjected to base harmonic excitation $x_0 = X_0 \sin \omega t$. Base excitation amplitude x_0 is provided by cam eccentricity and excitation frequency is varied by the change in the speed of the electrical drive motor.

The open circuit voltage V is measured across the copper coil terminals of SDOF VBEEH, at various excitation frequencies ω . The plot of V vs. ω is shown in Fig. 11a. The resistive electrical load R_L is connected across the copper coil terminals, and the voltage V_R across the load R_L is measured at different values of excitation frequency ω . R_L is varied from $R_L = 1000 \Omega$ to $R_L = 2000 \Omega$ using a resistive load bank developed for the same.

The power P_{aveh} that can be harvested from the SDOF VBEEH is estimated using the formula $P_{aveh} = V_R \times i_R$ where i_R is the current in the electrical load circuit and $i_R = \frac{V_R}{R_L}$. Therefore average power harvested is $P_{aveh} = \frac{V_R^2}{R_L}$, neglecting the internal resistance of the electrical copper

coil. R_L is varied as $R_L = 1000 \Omega$, $R_L = 1500 \Omega$, and $R_L = 2000 \Omega$. The plots of P_{aveh} vs. ω are obtained as shown in Fig. 11b. V_R , and P_{aveh} are maximum at resonant frequency $\omega = 33.5$ rad/s. These values fall sharply at off-resonance frequencies. At the power magnitude of 10 mw, the frequency band is (32.6–34.6) 2 rad/s. As such, it is necessary to modify the SDOF VBEEH in such a way that increased harvested power can be made available over a wide operational frequency band.

Experimental Analysis of Developed 2DOF VBEEH Device

For this purpose, harvester system (m_2, k_2, c_m, c_e) is mounted back in its place on the amplifier system (m_1, k_1). Now, this set-up is ready for experimental analysis of the developed 2DOF VBEEH device.

The developed 2 DOF VBEEH device is subjected to the base harmonic excitation $x_0(t) = X_0 \sin \omega t$ by the cam driven by an electric motor. The responses $x_2(t) = X_2 \sin \omega t$ of the harvester mass m_2 and $x_1(t) = X_1 \sin \omega t$ of the amplifier mass m_1 , at different frequencies of excitation, have been recorded using the strip chart recorder.

The open circuit voltage V across the copper coil terminals of TDOF VBEEH is measured at various frequencies of base excitation. The curves of V vs. ω are plotted as shown in Fig. 12.

The electrical load (pure resistive load R_L) is connected to the 2DOF VBEEH harvester and the voltage V_R across the resistance is measured at various values of frequencies of base excitation ω . R_L is varied as $R_L = 1000 \Omega$, $R_L = 1500 \Omega$, and $R_L = 2000 \Omega$. The curves of V_R vs. ω at various values of R_L are plotted as shown in Fig. 12.

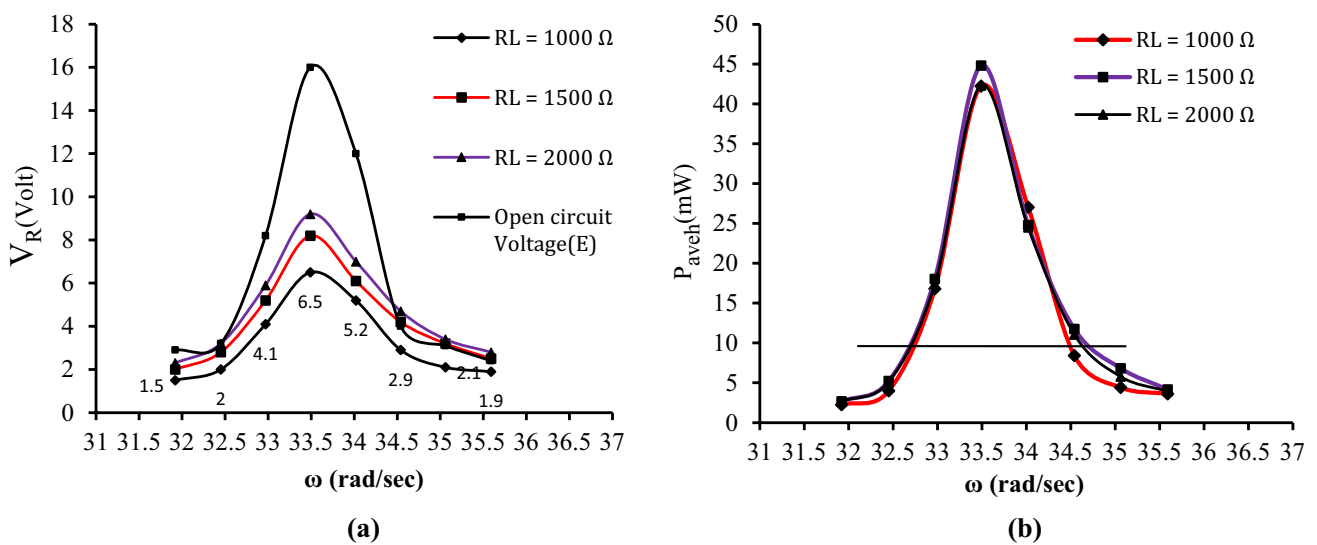


Fig. 11 a Voltage V_R vs. excitation frequency ω , b Harvested Power P_{aveh} vs. excitation frequency ω , for various values of R_L

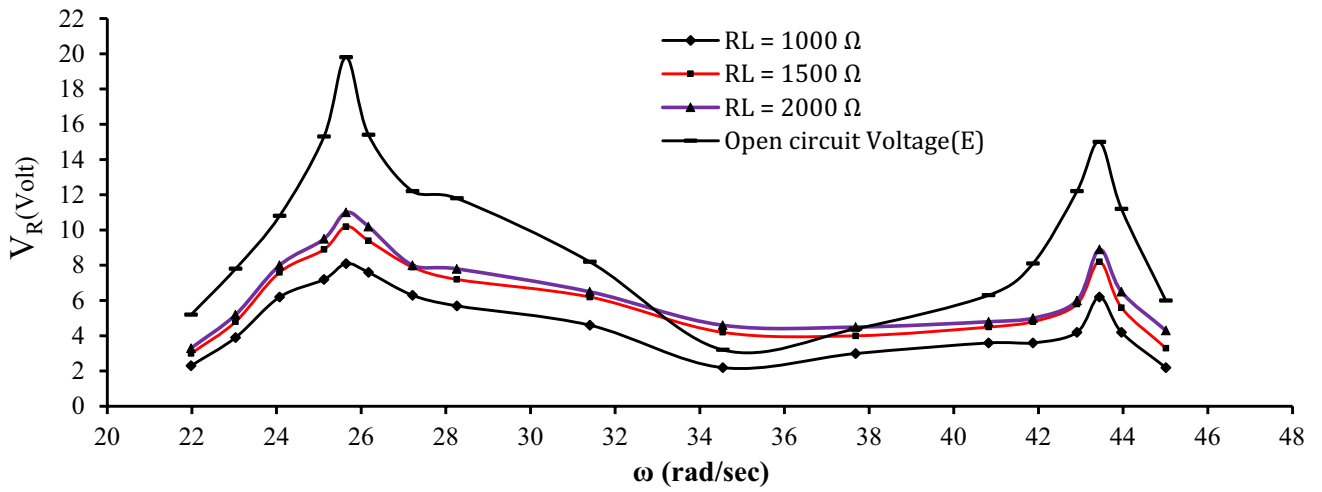


Fig. 12 Voltage V_R vs. excitation frequency ω for various values of R_L

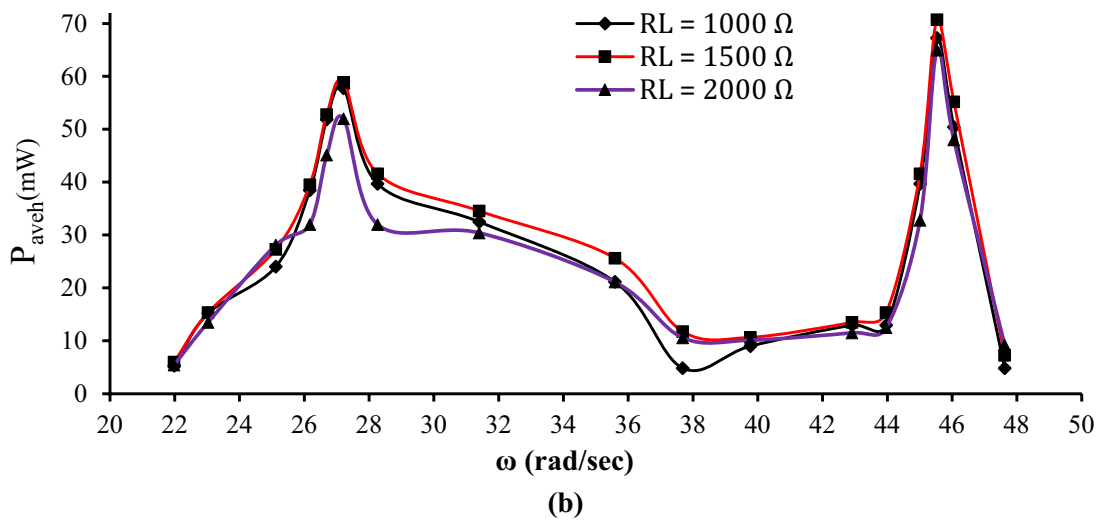
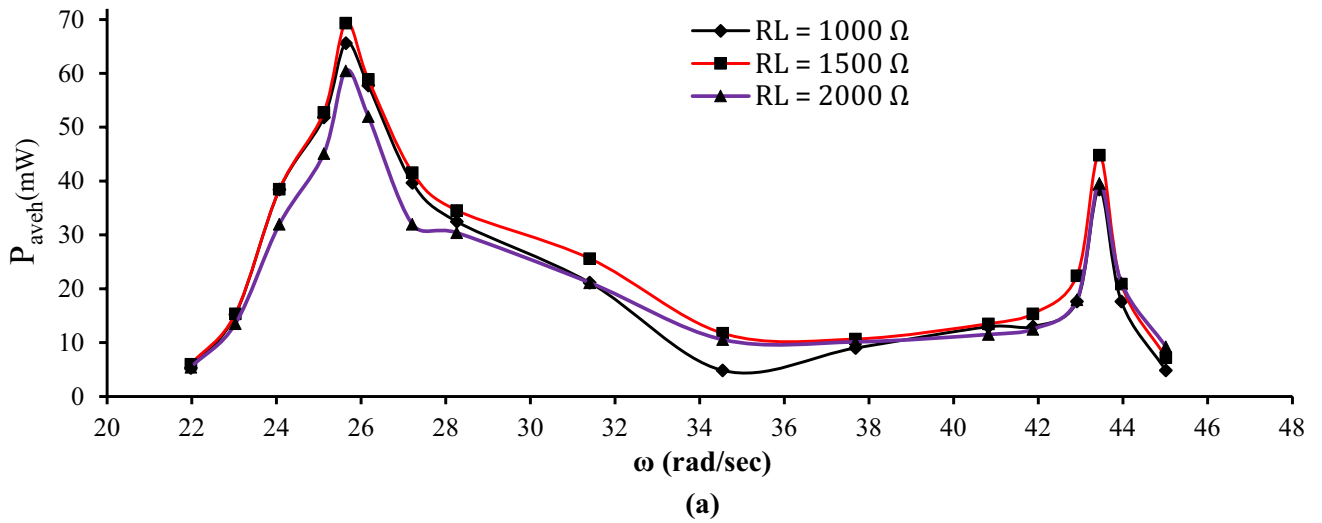


Fig. 13 Harvested power P_{aveh} vs. excitation frequency ω at various values of R_L **a** $\mu = 0.36$, **b** $\mu = 0.3$

The power P_{aveh} that can be harvested across resistive load R_L is calculated as $P_{aveh} = \frac{V_R^2}{R_L}$, at $R_L = 1000 \Omega$, $R_L = 1500 \Omega$, and $R_L = 2000 \Omega$ for various values of excitation frequency ω . The plots of P_{aveh} vs. ω are shown in Fig. 13.

From Fig. 13, it is clearly seen that the band width of operating excitation frequency has been increased. The values of relative displacement amplitude Z is maximum at two resonant frequencies indicating that the open circuit voltage V and voltage across the electric resistive load V_R will be available over a wide band of excitation frequency. This result shows that the harvester power P_{aveh} of a 2 DOF VBEEH is increased as compared to that of a SDOF VBEEH device. The power P_{aveh} is available over the wide band of excitation and the peak values of P_{aveh} are at the two resonant frequencies. It should be noted that the maximum values of P_{aveh} is available at a resistive load of 1500Ω which is approximately equal to internal resistance R_L of electrical copper coil.

From Fig. 13a and b, it is seen that the harvested power of 10 mw for mass ratio 0.36, the first mode band width = $B_{w1} = (34-23) = 11$ rad/s and second mode band width = $B_{w2} = (44-42) = 3$ rad/s. Total band width $B_w = B_{w1} + B_{w2} = 14$ rad/s compared to 2 rad/s of SdoF. For mass ratio 0.3, first mode band width = $B_{w1} = (37-23) = 14$ rad/s. Second mode band width = $B_{w2} = (47-44) = 3$ rad/s. Total band width $B_w = B_{w1} + B_{w2} = 17$ rad/s. The maximum power harvested is 45 mW, 70 mW and 60 mW, respectively, for SDoF, TDoF $\mu = 0.36$ and 0.3, respectively. It is clearly seen that the TDOF VBEEH bandwidth of operating excitation frequency and magnitude of harvested power has been increased as discussed in “Analysis of Single Degree of Freedom (SDoF) and Two Degree of Freedom (TDoF) Harvesters”.

Conclusions

In conclusion, the analysis and experimental results presented in this paper provide important insights for the design of Two-Degree-of-Freedom Vibration-Based Electromagnetic Energy Harvesters (TDOF VBEEHs). The derived expression for the non-dimensional power output of the TDOF VBEEH highlights the dependence on the selection of mass ratio (μ), tuning ratio (f), electrical damping ratio (ξ_e), and normalized excitation frequency (α). The values of μ and f are also linked to the effective non-dimensional bandwidth (BW). Therefore, careful consideration must be given to the choice of these parameters when designing a TDOF VBEEH, including the harvester mass-spring system and amplifier mass-spring system. The utilization of surface plots and contour diagrams proves to be an invaluable method for determining the global optimal power output of a TDOF VBEEH during the design phase. By simultaneously varying the values of the electrical damping ratio (ξ_e) and

normalized excitation frequency (α) for different values of the mass ratio (μ), the variation of non-dimensional power output (P_{aveh}^-) of the TDOF VBEEH can be studied. The results show that increased power output is attainable over a widened operational excitation frequency band compared to the traditional Single-Degree-of-Freedom (SDOF) VBEEH. Comparing the experimental and analytical results, it is evident that the TDOF VBEEH outperforms the SDOF VBEEH when the parameters are properly chosen. The experimental results show a maximum power harvested of 45 mW, 70 mW, and 60 mW for the SDOF VBEEH, TDOF VBEEH with $\mu = 0.36$, and TDOF VBEEH with $\mu = 0.3$, respectively. Additionally, the bandwidth achieved is 2 rad/s, 14 rad/s, and 17 rad/s for the SDOF VBEEH, TDOF VBEEH with $\mu = 0.36$, and TDOF VBEEH with $\mu = 0.3$, respectively. These findings highlight the superior performance and potential of TDOF VBEEHs over SDOF VBEEHs, emphasizing the importance of parameter selection in maximizing power output and widening the operational frequency band. The research results presented in this paper serve as valuable design guidelines for developing TDOF VBEEHs capable of powering small electronic devices when the amplitude and frequency data of the ambient vibration source are known.

Appendix 1

$$m_2 \ddot{x}_2 \uparrow = -k_2(x_2 - x_1) \downarrow - c(\dot{x}_2 - \dot{x}_1) \downarrow, \tag{11}$$

$$m_1 \ddot{x}_1 \uparrow = -k_2(x_1 - x_2) \downarrow - c(\dot{x}_1 - \dot{x}_2) \downarrow - k_1(x_1 - x_0) \downarrow, \tag{12}$$

where $c = c_m + c_e$, the relative displacement z between mass m_2 and mass m_1 is $z = x_2 - x_1$, hence, $\dot{z} = \dot{x}_2 - \dot{x}_1$ and $\ddot{z} = \ddot{x}_2 - \ddot{x}_1$. Substituting these values we get,

$$m_2 \ddot{z} + k_2 z + c \dot{z} = -m_2 \ddot{x}_1 \text{ and}, \tag{13}$$

$$m_1 \ddot{x}_1 + k_1 x_1 - k_2 z - c \dot{z} - k_1 x_0 = 0. \tag{14}$$

Take complex forms of variables as $z = Ze^{j\omega t}$, $x_1 = X_1 e^{j\omega t}$, and $x_0 = X_0 e^{j\omega t}$ then $\dot{z} = j\omega Z e^{j\omega t}$ and $\ddot{z} = -\omega^2 Z e^{j\omega t}$, $\dot{x}_1 = j\omega X_1 e^{j\omega t}$ and $\ddot{x}_1 = -\omega^2 X_1 e^{j\omega t}$.

Substituting these values in Eq. (13) we get Eq. (13) in the form

$$m_2 \omega^2 Z + k_2 Z + c(j\omega Z) = +m_2 \omega^2 X_1 \text{ or} \\ [(k_2 - m_2 \omega^2) + jc\omega] Z = m_2 \omega^2 X_1 \text{ then} \\ X_1 = \frac{[(k_2 - m_2 \omega^2) + jc\omega] Z}{m_2 \omega^2}. \tag{15}$$

Similarly, we get the Eq. (14) in the form

$$\begin{aligned} -m_1\omega^2 X_1 + k_1 X_1 - k_2 Z - cj\omega Z - k_1 X_0 &= 0 \\ (k_1 - m_1\omega^2)X_1 - (k_2 + cj\omega)Z &= k_1 X_0. \end{aligned} \quad (16)$$

Substituting value of X_1 , from Eq. (15) in Eq. (16) we get,

$$\begin{aligned} \left\{ (k_1 - m_1\omega^2) \left[\frac{(k_2 - m_2\omega^2) + jc\omega}{m_2\omega^2} \right] - (k_2 + cj\omega) \right\} Z &= k_1 X_0, \text{ or} \\ [(k_1 - m_1\omega^2)(k_2 - m_2\omega^2) + jc\omega(k_1 - m_1\omega^2) \\ - (k_2 + cj\omega)m_2\omega^2] Z &= m_2\omega^2 k_1 X_0, \end{aligned} \quad (17)$$

$$\begin{aligned} [k_1 k_2 - k_1 m_2 \omega^2 - k_2 m_1 \omega^2 + m_1 m_2 \omega^4 + jc\omega k_1 \\ - jc\omega m_1 \omega^2 - k_2 m_2 \omega^2 - cj\omega^3 m_2] Z &= k_1 m_2 \omega^2 X_0 \end{aligned}$$

$$\begin{aligned} \left\{ [k_1 k_2 - (k_1 m_2 + k_2 m_1 + k_2 m_2) \omega^2 + m_1 m_2 \omega^4] \right. \\ \left. + jc[\omega k_1 - (m_1 + m_2) \omega^3] \right\} Z &= k_1 m_2 \omega^2 X_0. \end{aligned} \quad (18)$$

Putting

$$\begin{aligned} a_1 &= [k_1 k_2 - (k_1 m_2 + k_2 m_1 + k_2 m_2) \omega^2 + m_1 m_2 \omega^4] \\ a_2 &= c[\omega k_1 - (m_1 + m_2) \omega^3] = (k_1 - (m_1 + m_2) \omega^2) c \omega, \text{ and} \\ a_3 &= k_1 m_2 \omega^2, \end{aligned}$$

we can rewrite Eq. (18) in the form as,

$$Z = \left(\frac{a_3}{a_1 + ja_2} \right) X_0 \text{ or } Z^2 = \left(\frac{a_3^2}{a_1^2 + a_2^2} \right) X_0^2. \quad (19)$$

Now, the average harvested power output P of 2DOF VBEEH is defined as

$$P = \text{Power output} = \int_0^v f dv,$$

where f is electromagnetic force induced in copper coil and magnet due to their relative velocity. We have $\dot{z} = (\dot{x}_2 - \dot{x}_1)$ hence $f = c_e \dot{z} = c_e (\dot{x}_2 - \dot{x}_1)$

using, this relation, the equation of the average power output P_{ave} is obtained as

$$P_{\text{ave}} = \int_0^z \dot{z} dz = \frac{1}{2} c_e [z^2] \text{ or } P_{\text{ave}} = \frac{1}{2} c_e (\dot{x}_2 - \dot{x}_1)^2. \quad (20)$$

Maximum Average Power output P_{ave} is given as,

$$P_{\text{ave}} = \frac{1}{2} c_e (\omega X_2 - \omega X_1)^2 \text{ or } P_{\text{ave}} = \frac{1}{2} c_e \omega^2 (X_2 - X_1)^2, \quad (21)$$

where X_2 and X_1 are amplitudes of $x_2(t)$ and $x_1(t)$ respectively.

Substituting $Z = (X_2 - X_1)$ in Eq. (19) and using the values of $a_1, a_2,$ and a_3 just defined.

We can write,

$$\begin{aligned} Z^2 &= (X_2 - X_1)^2 \\ &= \left[\frac{(k_1^2 m_2^2 \omega^4) X_0^2}{(k_1 k_2 - (k_1 m_2 + k_2 m_1 + k_2 m_2) \omega^2 + m_1 m_2 \omega^4)^2 + [(k_1 - (m_1 + m_2) \omega^2)]^2 c^2 \omega^2} \right]. \end{aligned} \quad (22)$$

Substituting Eq. (22) in Eq. (21), we get maximum average power output P_{ave} as

$$P_{\text{ave}} = \left[\frac{\frac{1}{2} c_e \omega^2 (k_1^2 m_2^2 \omega^4) X_0^2}{(k_1 k_2 - (k_1 m_2 + k_2 m_1 + k_2 m_2) \omega^2 + m_1 m_2 \omega^4)^2 + [(k_1 - (m_1 + m_2) \omega^2)]^2 c^2 \omega^2} \right]. \quad (23)$$

We have $c = c_m + c_e$, where $c_m = 2\zeta_m m_2 \omega_2$ and $c_e = 2\zeta_e m_2 \omega_2$ hence

$$c = 2(\zeta_m + \zeta_e) m_2 \omega_2 \text{ and } c^2 = 4(\zeta_m + \zeta_e)^2 m_2^2 \omega_2^2$$

Using the value of c^2 and c_e just defined, in Eq. (23), we can write,

$$P_{\text{ave}} = \left[\frac{\frac{1}{2} \times 2\zeta_e m_2 \omega_2 \omega^2 (k_1^2 m_2^2 \omega^4) X_0^2}{(k_1 k_2 - (k_1 m_2 + k_2 m_1 + k_2 m_2) \omega^2 + m_1 m_2 \omega^4)^2 + [(k_1 - (m_1 + m_2) \omega^2)]^2 4(\zeta_m + \zeta_e)^2 m_2^2 \omega_2^2 \omega^2} \right]. \quad (24)$$

The non-dimensional average power output $\overline{P_{\text{aven}}}$ can be written as,

$$\overline{P_{\text{aven}}} = \frac{P_{\text{ave}}}{X_0^2 \omega_1^3 m_1}, \tag{25}$$

where the term $X_0^2 \omega_1^3 m_1$ has the dimensions of the power.

Substituting Eq. (13) in Eq. (15), we get,

$$\overline{P_{\text{aven}}} = \left[\frac{\frac{\zeta_e m_2 \omega_2 \omega^2 k_1^2 m_2^2 \omega^4}{\omega_1^3 m_1}}{(k_1 k_2 - (k_1 m_2 + k_2 m_1 + k_2 m_2) \omega^2 + m_1 m_2 \omega^4)^2 + [(k_1 - (m_1 + m_2) \omega^2)]^2 4 (\zeta_m + \zeta_e)^2 m_2^2 \omega_2^2 \omega^2} \right]. \tag{26}$$

Consider the Numerator N of Eq. (26)

$$\begin{aligned} N &= \frac{\zeta_e m_2 \omega_2 \omega^2 k_1^2 m_2^2 \omega^4}{\omega_1^3 m_1} \\ N &= \frac{\zeta_e m_2}{m_1} \times \left(\frac{\omega_2}{\omega_1}\right) \left(\frac{\omega^2}{\omega_1^2}\right) (k_1^2 m_2^2 \omega^4) \\ N &= \zeta_e \mu f \alpha^2 (k_1^2 m_2^2 \omega^4) \\ N &= \zeta_e \mu f \alpha^2 (k_1^2 m_2^2 \omega^4) \left(\frac{\omega_1^4}{\omega_1^4}\right) \\ N &= \zeta_e \mu f \alpha^2 (k_1^2 m_2^2) \alpha^4 \omega_1^4 \\ N &= \zeta_e \mu f \alpha^6 k_1^2 m_2^2 \omega_1^4 \end{aligned}$$

where $\mu = \frac{m_2}{m_1}$ is the mass ratio, $f = \frac{\omega_2}{\omega_1}$ is the tuning ratio and $\alpha = \frac{\omega}{\omega_1}$ is the frequency ratio. Using the above value of numerator N of the Eq. (26) we get,

$$\begin{aligned} \overline{P_{\text{aven}}} &= \left[\frac{\zeta_e \mu f \alpha^6 k_1^2 m_2^2 \omega_1^4}{(k_1 k_2 - (k_1 m_2 + k_2 m_1 + k_2 m_2) \omega^2 + m_1 m_2 \omega^4)^2 + [(k_1 - (m_1 + m_2) \omega^2)]^2 4 (\zeta_m + \zeta_e)^2 m_2^2 \omega_2^2 \omega^2} \right] \\ \overline{P_{\text{aven}}} &= \left[\frac{\zeta_e \mu f \alpha^6}{\frac{(k_1 k_2 - (k_1 m_2 + k_2 m_1 + k_2 m_2) \omega^2 + m_1 m_2 \omega^4)^2}{k_1^2 m_2^2 \omega_1^4} + \frac{[(k_1 - (m_1 + m_2) \omega^2)]^2 4 (\zeta_m + \zeta_e)^2 m_2^2 \omega_2^2 \omega^2}{k_1^2 m_2^2 \omega_1^4}} \right] \\ &= \frac{\zeta_e \mu f \alpha^6}{\left[\frac{k_1 k_2}{k_1 m_2 \omega_1^2} - \left(\frac{k_1 m_2 + k_2 m_1 + k_2 m_2}{k_1 m_2 \omega_1^2} \right) \omega^2 + \left(\frac{m_1 m_2 \omega^4}{k_1 m_2 \omega_1^2} \right) \right]^2 + \left[\frac{k_1}{k_1 m_2 \omega_1^2} - \frac{(m_1 + m_2) \omega^2}{k_1 m_2 \omega_1^2} \right]^2 4 (\zeta_m + \zeta_e)^2 m_2^2 \omega_2^2 \omega^2} \\ &= \frac{\zeta_e \mu f \alpha^6}{D_1 + D_2}. \end{aligned} \tag{27}$$

Putting the values of D_1 and D_2 , as derived in Appendix I, 24, we get.

The non-dimensional output power $\overline{P_{\text{aven}}}$ of 2DOF VBEEH as

$$\overline{P}_{\text{aven}} = \frac{\zeta_e \mu f \alpha^6}{\left[\alpha^4 + f^2 - (1 + (1 + \mu)f^2)\alpha^2 \right]^2 + 4(\zeta_e + \zeta_m)^2 [f\alpha - (1 + \mu)f\alpha^3]^2} \quad (28)$$

Expression for D_1 and D_2 , we have,

$$\overline{P}_{\text{aven}} = \frac{\zeta_e \mu f \alpha^6}{\left[\frac{k_1 k_2}{k_1 m_2 \omega_1^2} - \left(\frac{k_1 m_2 + k_2 m_1 + k_2 m_2}{k_1 m_2 \omega_1^2} \right) \omega^2 + \left(\frac{m_1 m_2 \omega^4}{k_1 m_2 \omega_1^2} \right) \right]^2 + \left[\frac{k_1}{k_1 m_2 \omega_1^2} - \frac{(m_1 + m_2) \omega^2}{k_1 m_2 \omega_1^2} \right]^2 4(\zeta_m + \zeta_e)^2 m_2^2 \omega_2^2 \omega^2}$$

$$\overline{P}_{\text{aven}} = \frac{\zeta_e \mu f \alpha^6}{D_1 + D_2}$$

then

$$D_1 = \left[\frac{k_1 k_2}{\omega_1^2 k_1 m_2} - \left(\frac{k_1 m_2 + k_2 m_1 + k_2 m_2}{\omega_1^2 k_1 m_2} \right) \omega^2 + \left(\frac{m_1 m_2 \omega^4}{\omega_1^2 k_1 m_2} \right) \right]^2$$

$$= \left[\left(\frac{\omega_2}{\omega_1} \right)^2 - \left(\frac{1}{\omega_1^2} + \frac{\mu f^2}{\mu \omega_1^2} + \frac{\mu f^2}{\omega_1^2} \right) \omega^2 + \frac{1}{\omega_1^2} \frac{1}{\omega_1^2} (\omega)^4 \right]^2$$

$$= \left[f^2 - (1 + f^2 + \mu f^2) \frac{\omega^2}{\omega_1^2} + \frac{\omega^4}{\omega_1^4} \right]^2$$

$$= [f^2 - (1 + f^2 + \mu f^2)\alpha^2 + \alpha^4]^2, \quad (29)$$

$$D_2 = \left[\frac{k_1}{k_1 m_2 \omega_1^2} - \frac{(m_1 + m_2) \omega^2}{k_1 m_2 \omega_1^2} \right]^2 4(\zeta_m + \zeta_e)^2 m_2^2 \omega_2^2 \omega^2$$

$$= 4(\zeta_m + \zeta_e)^2 \left[\frac{k_1}{k_1 m_2 \omega_1^2} - \frac{(m_1 + m_2) \omega^2}{k_1 m_2 \omega_1^2} \right]^2 m_2^2 \omega_2^2 \omega^2$$

$$= 4(\zeta_m + \zeta_e)^2 \left[\frac{k_1 m_2 \omega_2 \omega}{k_1 m_2 \omega_1^2} - \frac{(m_1 m_2 \omega_2 \omega + m_2 m_2 \omega_2 \omega) \omega^2}{k_1 m_2 \omega_1^2} \right]^2$$

$$= 4(\zeta_m + \zeta_e)^2 \left[\frac{k_1 m_2 \omega_2 \omega}{k_1 m_2 \omega_1^2} - \left[\frac{m_1 m_2 \omega_2 \omega}{k_1 m_2 \omega_1^2} + \frac{(m_2 m_2 \omega_2 \omega)}{k_1 m_2 \omega_1^2} \right] \omega^2 \right]^2$$

$$= 4(\zeta_m + \zeta_e)^2 \left[\frac{\omega_2 \omega}{\omega_1 \omega_1} - \left[\frac{1}{\omega_1^2} \frac{\omega_2 \omega^3}{\omega_1^2} + \frac{m_2 k_2 (\omega_2 \omega^3)}{k_1 \omega_1^2} \right] \right]^2$$

$$= 4(\zeta_m + \zeta_e)^2 \left[f\alpha - \left[\frac{\omega_2}{\omega_1} \left(\frac{\omega}{\omega_1} \right)^3 + \frac{1}{\omega_2^2} \mu f^2 \frac{(\omega_2 \omega^3)}{\omega_1^2} \right] \right]^2$$

$$= 4(\zeta_m + \zeta_e)^2 \left[f\alpha - \left[f\alpha^3 + \mu f^2 \frac{\omega}{\omega_2} \left(\frac{\omega}{\omega_1} \right)^2 \right] \right]^2$$

$$= 4(\zeta_m + \zeta_e)^2 \left[f\alpha - \left[f\alpha^3 + \mu f^2 \frac{\omega}{\omega_1 \omega_2} \alpha^2 \right] \right]^2$$

$$= 4(\zeta_m + \zeta_e)^2 \left[f\alpha - \left[f\alpha^3 + \mu f^2 \alpha \frac{1}{f} \alpha^2 \right] \right]^2$$

$$= 4(\zeta_m + \zeta_e)^2 [f\alpha - [f\alpha^3 + \mu f\alpha^3]]^2$$

$$4(\zeta_m + \zeta_e)^2 [f\alpha - (1 + \mu)f\alpha^3]^2.$$

(30)

Appendix II

Calculation of First and Second Mode Natural Frequencies

If we remove electrical sub-system from 2DOF VBEEH and assume that the mechanical damping and electrical damping as zero i.e. $\zeta_m = \zeta_e = 0$, an undamped 2 DOF vibrating system results as shown in Fig. 3

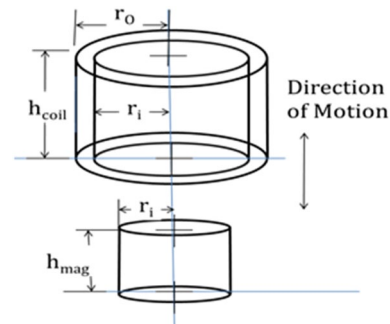


Fig. 14 Magnet and coil in-line combination

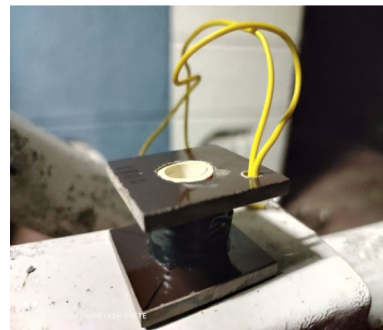


Fig. 15 Developed coil

Table 2 Specifications of the designed coil

| | | | | | |
|------------|----------------------------|-----|-----------|--|------|
| r_o | Coil outer radius (mm) | 10 | N_{lat} | Lateral turns of coil | 23 |
| r_i | Coil inner radius (mm) | 8 | N | Total number of turns of coil | 7790 |
| h_{coil} | Coil height (mm) | 30 | R_c | The internal resistance of the coil (Ω) | 1620 |
| N_{long} | Longitudinal turns of coil | 343 | L | The internal inductance of coil (H) | 0.45 |

Using well founded theory of vibration, we can write the equation of motion of mass m_2 as,

$$m_2\ddot{x}_2 = -k_2(x_2 - x_1) \text{ or}$$

$$m_2\ddot{x}_2 + k_2(x_2 - x_1) = 0. \tag{31}$$

Equation of motion of mass m_1 as

$$m_1\ddot{x}_1 = -k_2((x_1 - x_2) - k_1(x_1 - x_0))$$

$$m_1\ddot{x}_1 + k_1(x_1 - x_0) + k_2(x_1 - x_2) = 0.$$

For free vibration, set $x_0 = 0$, then equation of mass m_1 is

$$m_1\ddot{x}_1 + k_1x_1 + k_2(x_1 - x_2) = 0. \tag{32}$$

Setting $x_1 = X_1\sin\omega_n t$ and $x_2 = X_2\sin\omega_n t$ where, X_1 and X_2 are, respectively, the amplitudes of free vibration of mass m_1 and m_2 , ω_n is the circular natural frequency. Substitute $x_1(t)$ and $x_2(t)$ in Eqs. (31) and (32). Solving the Eqs. (31) and (32) for X_1 and X_2 . The frequency equation is obtained as

$$\omega_n^4 - \left[\frac{k_2}{m_2} + \frac{k_1}{m_1} + \frac{k_2}{m_1} \right] \omega_n^2 + \frac{k_1k_2}{m_1m_2} = 0. \tag{33}$$

Setting, Mass ratio = $\mu = \frac{m_2}{m_1}$, $\omega_2 = \sqrt{\frac{k_2}{m_2}}$, $\omega_1 = \sqrt{\frac{k_1}{m_1}}$, Tuning ratio = $f = \frac{\omega_2}{\omega_1}$ and substituting in Eq. (33), and after simplifying, we get

$$\frac{\omega_n^4}{\omega_1^4} - [1 + (1 + \mu)f^2] \frac{\omega_n^2}{\omega_1^2} + f^2 = 0. \tag{34}$$

Setting, $\frac{\omega_n^2}{\omega_1^2} = \overline{\omega}_n^2$ in non-dimensional form and solving the Eq. (34) for $\overline{\omega}_n^2$, we get the dimensionless undamped natural frequency equation as

$$\overline{\omega}_n^2 = \frac{[1 + (1 + \mu)f^2]}{2} \pm \sqrt{\left[\frac{1 + (1 + \mu)f^2}{2} \right]^2 - f^2}. \tag{35}$$

From the Eq. (35), we get, non-dimensional first mode frequency $\overline{\omega}_{n1}$, as

$$\overline{\omega}_{n1} = \sqrt{\frac{[1 + (1 + \mu)f^2]}{2}} - \sqrt{\left[\frac{1 + (1 + \mu)f^2}{2} \right]^2 - f^2}. \tag{36}$$

Non-dimensional second mode frequency $\overline{\omega}_{n2}$, as

$$\overline{\omega}_{n2} = \sqrt{\frac{[1 + (1 + \mu)f^2]}{2}} + \sqrt{\left[\frac{1 + (1 + \mu)f^2}{2} \right]^2 - f^2}. \tag{37}$$

It is seen from Eqs. (36) and (37) operational frequencies $\frac{\overline{\omega}_{n2} - \overline{\omega}_{n1}}$ depend on the mass ratio μ and tuning ratio f .

Appendix III

Selection of Magnet and Coil Design

- (i) Typically, four types of permanent magnets suitable for the coil-magnet system of a VBEEH are: Alnico, Ceramic, Samarium cobalt, and Neodymium Iron Boron (NdFeB). The properties such as high flux density and high magnetic field strength of NdFeB make it suitable for the coil-magnet system of VBEEH (Figs. 14, 15).

The dimensions of cylindrical NdFeB magnet selected for magnet-coil system are: diameter of magnet 10 mm and the height h_{mag} 30 mm and residual flux density $B_r = 1.4$ Tesla.

- (ii) The design of the coil is carried out according to the standard formulae [32]. These values are given in Table 2

Funding P V M acknowledges Vison Group on Science and Technology (Grant no. KSTePS/VGST-K-FIST L2/2078-L9 / GRD No.765) M I S acknowledges Vison Group on Science and Technology (Grant no. KSTePS/VGST-K-FIST L1/GRD No.387).

Data Availability The data that support the findings of this study are available from the corresponding author upon reasonable request.

Declarations

Conflict of Interest The authors declare that they have no conflict of interest.

References

1. Akinaga H (2020) Recent advances and future prospects in energy harvesting technologies. Jpn J Appl Phys 59(11):110201. <https://doi.org/10.3584/1347-4065/abbfa0>. (1-9)

2. Naifar S, Bradai S, Viehweger C, Kanoun O (2017) Survey of electromagnetic and magnetolectric vibration energy harvesters for low frequency excitation. *Measurement* 106:251–263. <https://doi.org/10.1016/j.measurement.2016.07.074>
3. Jiang J, Liu S, Feng L, Zhao D (2021) A review of piezoelectric vibration energy harvesting with magnetic coupling based on different structural characteristics. *Micromachines* 12(4):436. <https://doi.org/10.3390/mi12040436>. (1-34)
4. Ahmad MM, Khan FU (2021) Review of vibration-based electromagnetic– piezoelectric hybrid energy harvesters. *Int J Energy Res* 45(4):5058–5097. <https://doi.org/10.1002/er.6253>
5. Siang J, Lim M, Salman Leong M (2018) Review of vibration-based energy harvesting technology: Mechanism and architectural approach. *Int J Energy Res* 42(5):1866–1893. <https://doi.org/10.1002/er.3986>
6. Malaji PV, Friswell MI, Adhikari S et al (2022) High-energy orbit harvesting with torsionally coupled mistuned pendulums. *J Vib Eng Technol*. <https://doi.org/10.1007/s42417-022-00811-6>
7. Patil V, Sakri MI (2021) Experimental studies on the effect of shunted electrical loads on the performance of a vibration-based electromagnetic energy harvester. *FME Trans* 49:163–172. <https://doi.org/10.5937/fme2101163V>
8. Halim MA, Park JY (2015) Modeling and experiment of a handy motion driven, frequency up-converting electromagnetic energy harvester using transverse impact by spherical ball. *Sens Actuat A* 229:50–58. <https://doi.org/10.1016/j.sna.2015.03.024>
9. Halim MA, Cho H, Park JY (2015) Design and experiment of a human-limb driven, frequency up-converted electromagnetic energy harvester. *Energy Convers Manage* 106:393–404. <https://doi.org/10.1016/j.enconman.2015.09.065>
10. Zhang H, Corr LR, Ma T (2018) Effects of electrical loads containing non-resistive components on electromagnetic vibration energy harvester performance. *Mech Syst Signal Process* 101:55–66. <https://doi.org/10.1016/j.ymsp.2017.08.031>
11. Yildirim T, Ghayesh MH, Li W, Alici G (2017) A review on performance enhancement techniques for ambient vibration energy harvesters. *Renew Sustain Energy Rev* 71:435–449. <https://doi.org/10.1016/j.rser.2016.12.073>
12. Malaji P, Ali SF (2017) Broadband energy harvesting with mechanically coupled harvesters. *Sens Actuat A* 255:1–9. <https://doi.org/10.1016/j.sna.2016.12.003>
13. Caruso G (2015) Broadband energy harvesting from vibrations using magnetic transduction. *J Vib Acoust* 137(6):1–4. <https://doi.org/10.1016/j.sna.2016.12.003>
14. Zhu D, Roberts S, Tudor MJ, Beeby SP (2010) Design and experimental characterization of a tunable vibration-based electromagnetic microgenerator. *Sens Actuat A* 158(2):284–293. <https://doi.org/10.1016/j.sna.2010.01.002>
15. Sun K, Liu GQ, Xu XY (2012) In *Applied Mechanics and Materials*, vol. 130. Trans Tech Publ, pp 2778–2782. <https://doi.org/10.4028/www.scientific.net/AMM.130-134.2778>
16. Aldraihem O, Baz A (2011) Energy harvester with a dynamic magnifier. *J Intell Mater Syst Struct* 22(6):521–530. <https://doi.org/10.1177/1045389X11402706>
17. Zhou W, Penamalli GR, Zuo L (2011) An efficient vibration energy harvester with a multi-mode dynamic magnifier. *Smart Mater Struct* 21(1):015014. <https://doi.org/10.1088/0964-1726/21/1/015014>. (1-9)
18. Zorlu O, Topal ET, Külah H (2010) A vibration-based electromagnetic energy harvester using mechanical frequency up-conversion method. *IEEE Sens J* 11(2):481–488. <https://doi.org/10.1109/JSEN.2010.2059007>
19. Malaji P, Friswell M, Adhikari S, Litak G (2020) Enhancement of harvesting capability of coupled nonlinear energy harvesters through high energy orbits. *AIP Adv* 10(8):085315. <https://doi.org/10.1063/5.0014426>. (1-6)
20. Malaji P, Ali S, Adhikari S, Friswell M (2016) Analysis of harvesting energy from mistuned multiple harvesters with and without coupling. *Procedia Eng* 144:621–628. <https://doi.org/10.1016/j.proeng.2016.05.052>
21. Chaurha A, Malaji P, Mukhopadhyay T (2022) Dual functionality of vibration attenuation and energy harvesting: effect of gradation on non-linear multiresonator metastructures. *Eur Phys J Special Topics* 231(8):1403–1413. <https://doi.org/10.1140/epjs/s11734-022-00506-9>
22. Tao K, Wu J, Tang L, Xia X, Lye SW, Miao J, Hu X (2016) A novel two-degree-of-freedom mems electromagnetic vibration energy harvester. *J Micromech Microeng* 26(3):035020. <https://doi.org/10.1088/0960-1317/26/3/035020>. (1-12)
23. Chen SJ, Wu JY (2016) Fabrication of a 2-dof electromagnetic energy harvester with in-phase vibrational bandwidth broadening. *Smart Mater Struct* 25(9):095047. <https://doi.org/10.1088/0964-1726/25/9/095047>
24. Tang X, Zuo L (2011) Enhanced vibration energy harvesting using dual-mass systems. *J Sound Vib* 330(21):5199–5209. <https://doi.org/10.1016/j.jsv.2011.05.019>
25. Tai WC, Zuo L (2017) On optimization of energy harvesting from base-excited vibration. *J Sound Vib* 411:47–59. <https://doi.org/10.1016/j.jsv.2017.08.032>
26. Smilek J, Hadas Z (2017) Coil optimization for linear electromagnetic energy harvesters with non-uniform magnetic field. *Adv Intell Syst Comput* 644:734–742
27. Kim SC, Kim JG, Kim YC, Yang SJ, Lee H (2019) A study of electromagnetic vibration energy harvesters: design optimization and experimental validation. *Int J Precis Eng Manuf Green Technol* 6:779–788. <https://doi.org/10.1007/s40684-019-00130-4>
28. Maroofiazar R, Fahimi Farzam M (2022) A hybrid vibration energy harvester: experimental investigation, numerical modeling, and statistical analysis. *J Vib Eng Technol*. <https://doi.org/10.1007/s42417-022-00658-x>
29. Wang W, Zhang Y, Bowen CR, Wei ZH, Cao J (2022) Energy harvesting from ultra-low-frequency vibrations through a quasi-zero stiffness electromagnetic energy harvester. *J Vib Eng Technol*. <https://doi.org/10.1007/s42417-022-00658-x>
30. Liu Y, Zhan W, Xing M, Wu Y, Xu R, Wu X (2022) Boundary control of a rotating and length-varying flexible robotic manipulator system. *IEEE Trans Syst Man Cybern* 52(1):377–386. <https://doi.org/10.1109/TSMC.2020.2999485>
31. Liu Y, Fu Y, He W, Hui Q (2019) Modeling and observer-based vibration control of a flexible spacecraft with external disturbances. *IEEE Trans Industr Electron* 66(11):8648–8658. <https://doi.org/10.1109/TIE.2018.2884172>

Publisher's Note Springer Nature remains neutral with regard to jurisdictional claims in published maps and institutional affiliations.

Springer Nature or its licensor (e.g. a society or other partner) holds exclusive rights to this article under a publishing agreement with the author(s) or other rightsholder(s); author self-archiving of the accepted manuscript version of this article is solely governed by the terms of such publishing agreement and applicable law.